International Journal of Multiphase Flow 35 (2009) 1067–1076

Contents lists available at ScienceDirect

International Journal of Multiphase Flow

journal homepage: www.elsevier.com/locate/ijmulflow

Review

Review of nucleate pool boiling bubble heat transfer mechanisms ☆

Jungho Kim *

University of Maryland, Department of Mechanical Engineering, College Park, MD 20742, United States

ARTICLE INFO

Article history:
Received 15 June 2009
Received in revised form 27 July 2009
Accepted 31 July 2009
Available online 6 August 2009

Keywords:
Boiling
Bubbles
Heat transfer mechanisms

ABSTRACT

Enhanced convection, transient conduction, microlayer evaporation, and contact line heat transfer have all been proposed as mechanisms by which bubbles transfer energy during boiling. Models based on these mechanisms contain fitting parameters that are used to fit them to the data, resulting a proliferation of "validated" models. A review of the recent experimental, analytical, and numerical work into single bubble heat transfer is presented to determine the contribution of each of the above mechanisms to the overall heat transfer. Transient conduction and microconvection are found to be the dominant heat transfer mechanisms. Heat transfer through the microlayer and at the three-phase contact line do not contribute more than about 25% of the overall heat transfer.

1. Introduction

Boiling is a complex process in which mass, momentum, and energy transfer (single and two-phase) involving a solid wall, liquid, and vapor are tightly coupled. Consider a bubble nucleating, growing, and departing from a single site on a heated surface. The bubble is assumed to nucleate when the superheated liquid layer above the site grows sufficiently thick to cause the vapor/gas trapped within the cavity to overcome the surface tension force and grow according to the theory of Hsu (1962). We are not concerned here with details of the nucleation process, but only with how a bubble growing on a heated surface removes energy.

Once a bubble nucleates, it grows through evaporation of liquid at the liquid/vapor interface. Numerous mechanisms are available through which energy is transferred from the wall as illustrated in Fig. 1a. A quickly growing, hemispherically shaped bubble can trap a thin layer of liquid between the growing bubble and the superheated wall (the microlayer), and evaporation of this liquid contributes to bubble growth (q_{ml}). The energy to evaporate this liquid comes from the energy stored in the superheated wall. Liquid can also grow through evaporation of the superheated liquid layer surrounding the bubble cap (q_{sl}) (e.g., Van Stralen 1966a,b; Van Stralen 1967). Inertially controlled growth occurs when the heat transfer to the interface is very fast and the bubble growth is limited by the rate at which momentum can be transferred to the surrounding liquid. Thermally controlled growth occurs when the bubble growth is limited by the rate at which heat can be conducted to the liquid/vapor interface. Another mechanism for bubble growth is through evaporation at the three-phase contact line (q_{cl}) once a dry patch forms on the surface due to partial dryout of the microlayer (Fig. 1a). The growing bubble can also perturb the liquid adjacent to the bubble and disrupt the background natural convection boundary layer (q_{nc}), resulting in energy transfer by microconvection (q_{mc}).

As the bubble grows, the buoyancy force continues to increase and can initiate the bubble departure process. The available heat transfer mechanisms as the bubble departs are illustrated in Fig. 1b. Heat transfer through the microlayer (q_{ml}) can still occur if it has not completely dried out. Energy from the superheated liquid layer (q_{sl}) can continually be added through the bubble cap, especially if the bulk liquid is not subcooled. If a dry patch has formed on surface due to partial dryout of the microlayer during bubble growth, the dry patch will be rewet with liquid as the bubble departs. Heat transfer occurs at the three-phase contact line (q_{cl}), but this heat transfer is expected to be smaller than the heat transfer during bubble growth since the advancing contact angle is steeper than the receding contact angle, resulting in a thicker liquid layer on the surface. Transient conduction into the advancing liquid front occurs as the dry patch is rewet (q_{tc}). The departing bubble can perturb the liquid adjacent to the bubble resulting in energy transfer by microconvection (q_{mc}). The vortices in the wake of the departing bubble can cause additional microconvection and reduce the thickness of the superheated liquid layer.

Due to the many possible heat transfer mechanisms, it is not surprising that the mechanisms by which individual bubbles transfer heat have been debated over many decades, resulting in the emergence of many competing, mutually exclusive models. The use of relatively large, thermally massive heaters compared to the departing bubbles in the vast majority of experimental work have resulted in time averaged and space averaged heat transfer measurements to be obtained –local, time resolved heat transfer

☆ This paper was originally presented at the ASME 2009 INCMM Conference in Pohang, Korea.

* Tel.: +1 301 405 5437.
E-mail address: kimjh@umd.edu.

0301-9322/$ - see front matter © 2009 Elsevier Ltd. All rights reserved.
doi:10.1016/j.ijmultiphaseflow.2009.07.008

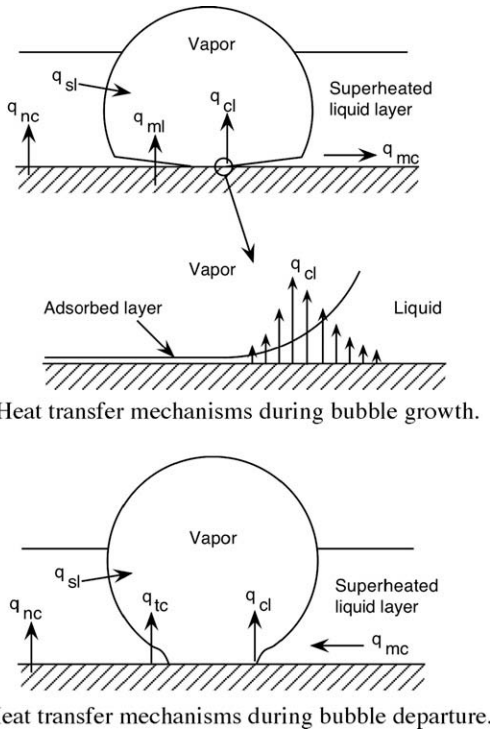

Fig. 1. Bubble heat transfer mechanisms.

data were not available to confirm details of the models. These experiments usually used a single heating element operated at constant heat flux, making it difficult to obtain information about local temperature variations underneath bubbles. Other experiments utilized surfaces held at constant temperature averaged over the entire heater, but the local heat flux and temperature were not measurable and could vary significantly across the heater. Within the past few years, however, numerous experiments have been performed in which detailed, local measurements of the wall heat transfer throughout the bubble growth and departure process have been obtained, allowing details of the models to be tested. Detailed numerical simulations of the bubble growth and departure process have also appeared. The purpose of this paper is to review the recent literature and clarify the contributions of the various bubble heat transfer mechanisms.

2. Review of bubble heat transfer models

Many of the early models were based on bubble agitation/microconvection being the primary heat transfer mechanism. These models did not include phase change, but relied on an analogy with forced convection, i.e., the role of the bubble was to change the length and velocity scales used to correlate data (e.g., Rosenhow 1952; Forster and Zuber, 1955; Forster and Greif 1959; Zuber 1963; Tien 1962). For example, the vapor–liquid exchange model proposed by Forster and Greif (1959) assumed that bubbles act as micropumps that remove a quantity of hot liquid from the wall equal to a hemisphere at the maximum bubble radius, replacing it with cold liquid from the bulk. The heat transferred from a single site was the energy required to heat this volume of liquid from the bulk temperature to the average of the wall and bulk temperatures.

2.1. Transient conduction model (TC)

Building on the work of Han and Griffith (1965), Mikic and Rohsenhow (1969) developed a model of bubble heat transfer that assumed a departing bubble scavenges away the superheated layer surrounding the bubble over an area twice the bubble departure diameter, allowing colder bulk liquid to contact the surface (Fig. 2). No wall heat transfer was assumed during the bubble growth process. The superheated layer is only renewed during the waiting time (the time after bubble departure and before nucleation of a new bubble) by transient conduction into a semi-infinite liquid. Transient conduction into this bulk liquid after bubble departure was assumed to be the dominant mode of heat transfer.

If this model were correct, we would expect to observe a very large, spatially uniform heat transfer immediately after bubble departure over an area about twice the bubble departure diameter that would then decay during regrowth of the superheated liquid layer. The heat transfer during the bubble growth and departure process would be negligible.

2.2. Microlayer heat transfer model (ML)

Snyder and Edwards (1956) first suggested that growing bubbles could trap a thin layer of liquid at the wall which could then evaporate and transfer substantial amounts of energy. Moore and Mesler (1961) measured temperature fluctuations on the wall under bubbles during nucleate boiling. Hendricks and Sharp (1964) correlated the wall temperature fluctuations with high-speed videos of individual bubbles and showed that the rapid temperature decrease in the wall temperature was associated with bubble growth. Cooper and Lloyd (1969) obtained temperature measurements during boiling of toluene and isopropyl alcohol on glass and ceramic substrates whose backsides were radiantly heated. Both surfaces were instrumented with thin film thermocouples that were less than 0.5 μm thick. A typical bubble grew hemispherically forming a microlayer on the surface. Their results are shown in Fig. 3. Temperature–time data indicated an initial sharp drop in temperature as the microlayer evaporated, a recovery in temperature after formation of a dry spot, then a small drop in temperature and subsequent recovery as liquid rewet the surface during bubble departure. The heat flux deduced from these temperature–time curves by integration of the heat conduction equation indicated large heat transfer during microlayer evaporation and a much smaller heat transfer during rewetting of the surface. They argued that the initial thickness of the microlayer varied according to

$$\delta_0 = C_2\sqrt{\nu_l t_g} \tag{1}$$

where $C_2 = 0.8$, ν_l is the liquid kinematic viscosity, and t_g is the time required for the microlayer to form. Comparison of the observed

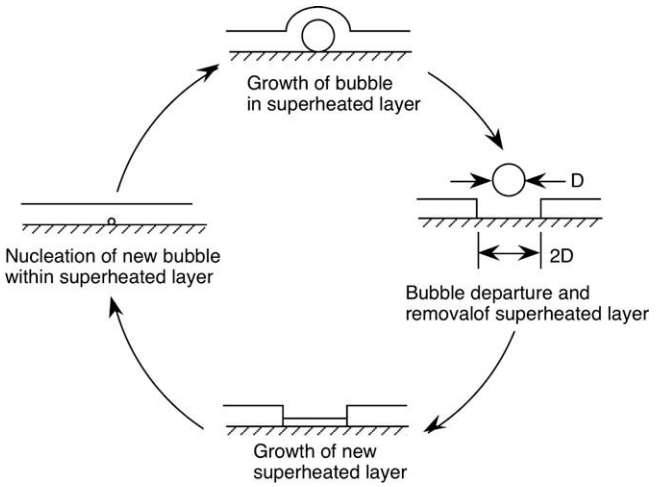

Fig. 2. Bubble heat transfer mechanism suggested by Mikic and Rohsenhow (1969).

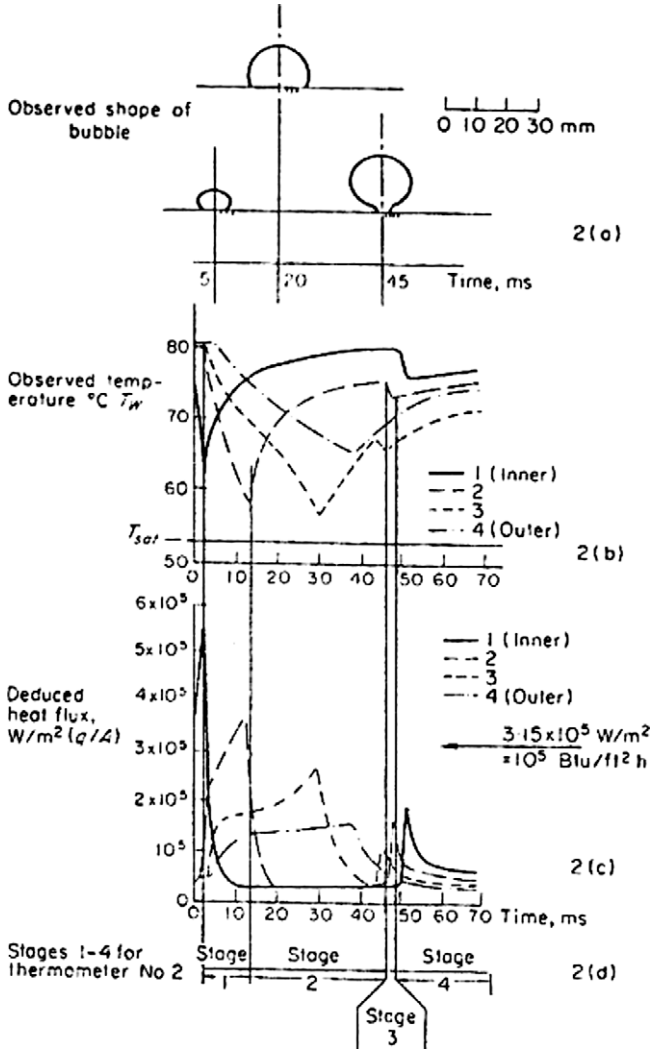

Fig. 3. Wall temperature and heat flux results. From Cooper and Lloyd (1969).

bubble volume with the volume evaporated from the microlayer was within 17% for a saturated fluid, indicating that bubble gained most of its energy through microlayer evaporation. It should be noted that the bubbles were quite large (20–30 mm diameter) with long growth time (~50 ms).

This model predicts a high heat transfer under the bubble during bubble growth as the microlayer evaporates (the highest heat transfer would occur where the microlayer is thinnest just next to the perimeter of the dry patch), and negligible heat transfer outside of the bubble footprint. The heat transfer during the bubble departure process should only be limited to the evaporation of the residual microlayer and there should be little heat transfer as the dry patch is rewet with liquid. The bubble volume should be obtainable from the microlayer evaporation.

2.3. Contact line heat transfer model (CL)

This model by Stephan and Hammer (1994) assumes that the dominant mode of heat transfer is due to the evaporation of a thin liquid meniscus at the three-phase contact line. Although the extent of the meniscus is small, the heat transfer through the thin liquid film can be very high (Wayner et al., 1976). The meniscus in the vicinity of the contact line can become very thin due to stretching of the meniscus, resulting in high heat transfer in this region. The adsorbed layer is usually just a few molecules thick and cannot be evaporated due to molecular adhesion forces. This force decreases rapidly with film thickness ($F_a \propto \delta^{-4}$), however, and heat transfer by conduction across the liquid film occurs due to the temperature difference ($T_w - T_{sat}$). An optimum in the heat transfer occurs when the film becomes thick enough such that the adhesion forces become small, yet thin enough so the heat conduction through the film is high. At larger film thicknesses, the conduction resistance dominates, resulting in lower heat transfer. The contact angle corresponds to the receding contact angle.

Stephan and Hammer (1994) constructed a model in which heat could be transferred through the microregion (the three-phase contact line) and the macro-region (the liquid adjacent to the microregion and the wall) of a growing bubble. Capillary pressure and curvature effects were included in the microregion model. Results were obtained for boiling of R-114 on a copper plate. For a single bubble of radius 0.125 mm and wall superheat of 3.5 K, the extent of the microregion was found to be less than 1 μm, but accounted for about 38% of the total heat transfer. A peak heat flux of 1550 W/cm^2 was observed within the microregion. When the superheat was increased to 4.2 K, about 60% of the heat passed through the microregion.

If this model is correct, an extremely high heat transfer should be observed at the three-phase contact line over a distance of $\sim 10^{-6}$ m, and much lower heat transfer should occur in the macro-region. It also predicts that the contact line heat transfer should be higher as the bubble grows than when the surface is rewet by liquid during bubble departure since the contact angle corresponds to a shallower receding contact angle (θ_r) instead of the larger advancing contact angle (θ_a).

2.4. Comparison of models

Since the heat transfer signatures of each of the above models are quite distinct, comparison with the local heat transfer data from recent experiments and simulations provides a unique opportunity to evaluate the merits of the above models. In the remainder of this paper, the recent experimental, analytical, and numerical data in which detailed, local measurements of the wall heat transfer throughout the bubble formation and departure process were obtained are reviewed and evaluated. The heat transfer signatures provided in these studies can be combined with visual observations of bubble growth deduce the correct heat transfer mechanisms.

3. Experiments

3.1. Microheater array data

Yaddanapuddi and Kim (2001) used a microheater array consisting of 96 independently controlled heaters each nominally 0.27×0.27 mm^2 in size to measure the heat transfer distribution under isolated bubbles. The heaters were kept at constant temperature through the use of analog electronic feedback circuits and the power required to do this was measured. The frequency response of the circuit and heater combination was measured to be 15 kHz. Demiray and Kim (2004) performed similar measurements, but using a microheater array with individual heaters that were nominally 0.1×0.1 mm^2 in size.

The evolution of a bubble is shown in Fig. 4, where the individual heaters in the array have been colored according to the heat transfer. The size and shape of the bubble can be inferred from the dark ring shown in the images as shown in the schematic. The outer diameter of the ring corresponds to the projected diameter of the bubble, while the inner diameter gives an idea of the

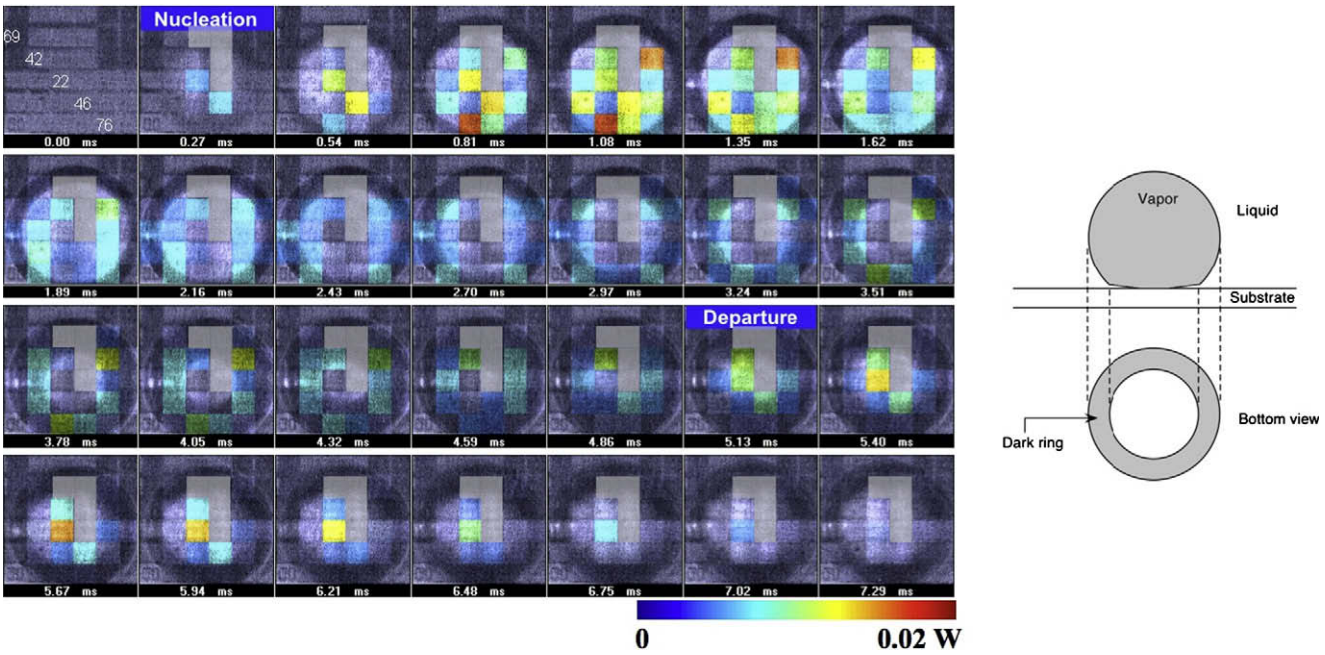

Fig. 4. Single FC-72 bubble (bubble L1) growing on a wall (T_{wall} = 76 °C, T_{sat} = 57 °C, T_{bulk} = 52 °C). From Demiray and Kim (2004).

shape of the bubble. A thin, dark ring corresponds to a hemispherical bubble, while a ring whose thickness is equal to the bubble radius indicates a spherical bubble. Nucleation occurs between 0 and 0.27 ms. The bubble grows to it largest outer diameter between 1.62 and 1.89 ms after nucleation. The bubble shape appears to be approximately hemispherical as indicated by the thin, dark ring. A large increase in the heat transfer under almost the entire bubble is observed during this time, consistent with evaporation from a microlayer between the bubble and the wall. Starting from 1.89 ms, the development of a low heat transfer region at the center of the bubble is observed, indicating progressive dryout of the microlayer. The dry spot size, as evidenced by the inner circle, reaches a maximum at 3.51 ms. The bubble departure process begins at about 1.89 ms as indicated by a decrease in the inside diameter of the ring, eventually rewetting the dry spot completely. Higher heat transfer is observed on the center heaters as they are rewet by the bulk liquid. Bubble departure occurs at 5.13 ms, and is associated with a spike in heat transfer at the center heaters that then decays with time.

The area averaged heat transfer due to bubble nucleation, growth, and departure for this bubble as well as others are shown in Fig. 5. Bubbles L1 and L2 were preceded by a relatively long waiting period. Both these bubbles are associated with a sharp peak in the wall heat transfer at $t \sim 1.2$ ms which is consistent with the formation and evaporation of a microlayer between the bubble and the wall. The heat transfer decays with time as the bubble rewets the surface and departs and continues to decay after bubble departure as the superheated thermal boundary layer is regenerated.

The wall heat transfer data shown in Fig. 5 can be used to compute an equivalent bubble diameter (d_{eq}) by assuming that the heat transferred from all of the heaters through contact line heat transfer and microlayer evaporation appears as latent heat:

$$\rho_v \frac{\pi d_{eq}^3(t)}{6} h_{fg} = \int_0^t q''_h A_h \, dt \tag{2}$$

where time t = 0 is assumed to be the start of nucleation for a single bubble. The bubble is assumed to be full of vapor at the prevailing pool pressure. The equivalent diameter is plotted in Fig. 6 along with the measured bubble diameter. It is seen that d_{eq} is significantly smaller than the physical bubble diameter during the bubble growth time, indicating the heat transferred from the wall cannot account for the bubble growth alone. For example, bubbles L5 and L6 reach a diameter of 0.5 mm in 0.54 ms. If a hemispherical bubble shape is assumed during this early bubble growth period, the diameter of a spherical bubble of equivalent volume is 0.4 mm. This is over twice as large as the d_{eq} derived from the wall heat transfer measurements, indicating that the wall heat transfer due to microlayer evaporation (q_{ml}) and contact line heat transfer (q_{cl}) could have contributed at most $(\frac{1}{2})^3$ or 12.5% of the energy required to produce the bubble. The bubble must have gained the balance of its energy from the superheated liquid layer surrounding it. The superheated liquid layer thus acts as a reservoir of energy from

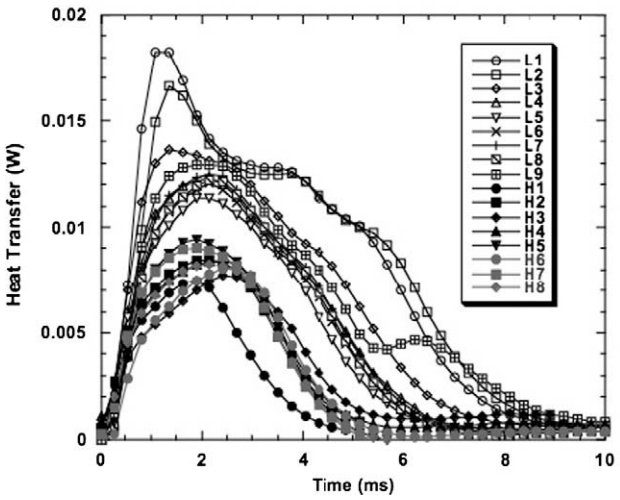

Fig. 5. Heat transfer from the microheater array for a series of bubble nucleating on the heater. Bubble preceded by an L were obtained with: T_{wall} = 76 °C, T_{sat} = 57 °C, T_{bulk} = 52 °C). Bubble preceded by an H were obtained with: T_{wall} = 76 °C, T_{sat} = 57 °C, T_{bulk} = 41 °C). From Demiray and Kim (2004).

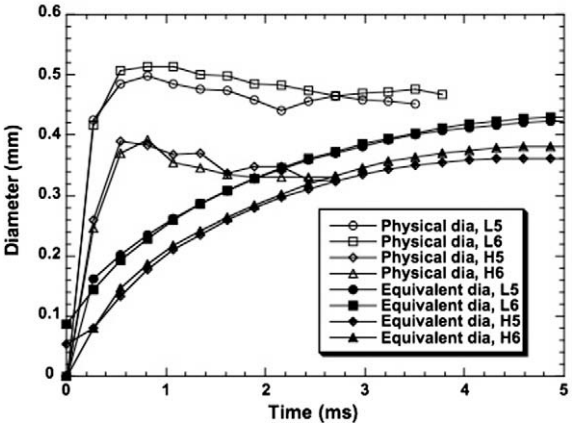

Fig. 6. Comparison of physical and equivalent bubble diameters. From Demiray and Kim (2004).

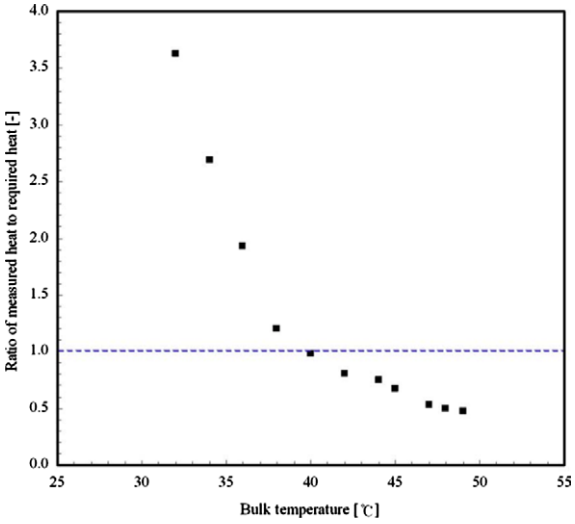

Fig. 7. Ratio of measured wall heat transfer to heat required to grow bubble to observed size. From Kim et al. (2006).

which the bubble draws during its growth. Conduction and microconvection during bubble growth and after bubble departure are the mechanisms through which this energy is replenished. Heat transfer measurements and comparison with a simple model under sliding and oscillating bubbles also indicated that transient conduction during the rewetting process is dominant (see Demiray and Kim 2004 for details).

Myers et al. (2005) operated a microheater array in constant heat flux mode to investigate the effect of thermal boundary condition on the heat transfer mechanisms. Each heater in the array dissipated the same heat flux, and the temperature variation of the heaters were measured. A 3-D, transient, finite difference numerical simulation was used to compute the instantaneous temperature distribution within the substrate from which the temperature gradient at the wall, and thus the substrate conduction, was computed. The substrate conduction was then subtracted from the heater power to obtain the local wall-to-liquid heat transfer. The data indicated that most of the energy required for bubble growth came from the superheated liquid layer around the bubble. Microlayer evaporation and contact line heat transfer accounted for no more than 23% of the total heat transferred from the surface. The dominant heat transfer mechanism was transient conduction and/or microconvection into the liquid during bubble departure.

Similar observations were made by Lee et al. (2003a,b) using R11 as the working fluid. They obtained the bubble volume from side view images of the bubble shape, and assumed changes in the bubble shape were due to evaporation of liquid:

$$\dot{q} = \dot{m} h_{fg} = 4\pi \rho_v h_{fg} R^2 \frac{dR}{dt} \tag{3}$$

The heat transfer rate was measured using a microheater array. The heat flow required to grow the bubble to the observed size was found to be approximately twice as large as the heat transfer from the wall, indicating that the additional heat required must have been supplied through another surface (the liquid–vapor interface). Kim et al. (2006) made additional measurements using R113 (T_{sat} = 47.6 °C) at various bulk fluid temperatures. They computed the ratio of measured wall heat transfer to the heat transfer required to grow the bubble to the observed size for superheated, saturated, and subcooled bulk fluid temperatures (Fig. 7). When the bulk liquid was superheated (T_{bulk} = 49 °C), the ratio was 0.44, indicating additional heat must have been supplied through the liquid–vapor interface. As the bulk temperature decreased, the ratio increased, reaching as high as 3.6 at a bulk temperature of 32.2 °C as a result of condensation at bubble cap. The bulk fluid temperature at which the required and measured heat balanced was 40 °C.

3.2. Micro heat flux sensor data

Moghaddam and Kiger (2008) obtained measurements under isolated bubbles of FC-72 growing from an artificial nucleation site. Surrounding the nucleation site were two layers of temperature sensors separated by an insulator (BCB) that enabled measurement of local heat flux with a resolution of 22–40 μm. Bubbles with and without a waiting time between nucleation events occurred when the wall temperature was set at 80.5 °C, while bubbles without waiting time occurred at 86.4 °C, 91.4 °C, and 97.2 °C. Their measurements indicated that microlayer heat transfer accounted for between 16.3% and 28.8% of the total heat transfer, and the combination of transient conduction and microconvection was the remainder for the cases without waiting time between bubbles. In those cases with waiting time, the microlayer contributed 26.5% and the balance of the heat transfer was through transient conduction and microconvection, confirming the results obtained using the microheater array. By measuring the heat transfer outside of the bubble projected area during boiling, and comparing to cases where no boiling occurred on the surface, they were able to separate out the contribution of natural convection and microconvection induced by bubble motion. They observed that the microconvection contribution became increasingly important as the wall temperature increased (Fig. 8). They concluded that evaporation at the three-phase contact line it was about 2–3 orders of magnitude less than their measured heat transfer and was therefore negligible.

3.3. Liquid crystal data

Unencapsulated liquid crystals applied to the backside of thin, electrically heated metallic plates have been used by numerous researchers to obtain temperature distributions during nucleate boiling (e.g., Watwe and Hollingsworth 1994; Bayazit et al., 2003; Kenning et al., 2001; Sodtke et al., 2006). Typically, the hue component vs. temperature is obtained from an in-situ calibration which also takes into account changes with viewing angle. To obtain high resolution temperature data, narrow-band liquid crystal must be used, but this limits the temperature range that can be measured. Mixtures of liquid crystal formulations with differing colorplay range could be applied as a thicker layer to extend the range at the expense of frequency response. An additional time delay on the order of a few milliseconds or longer can result since

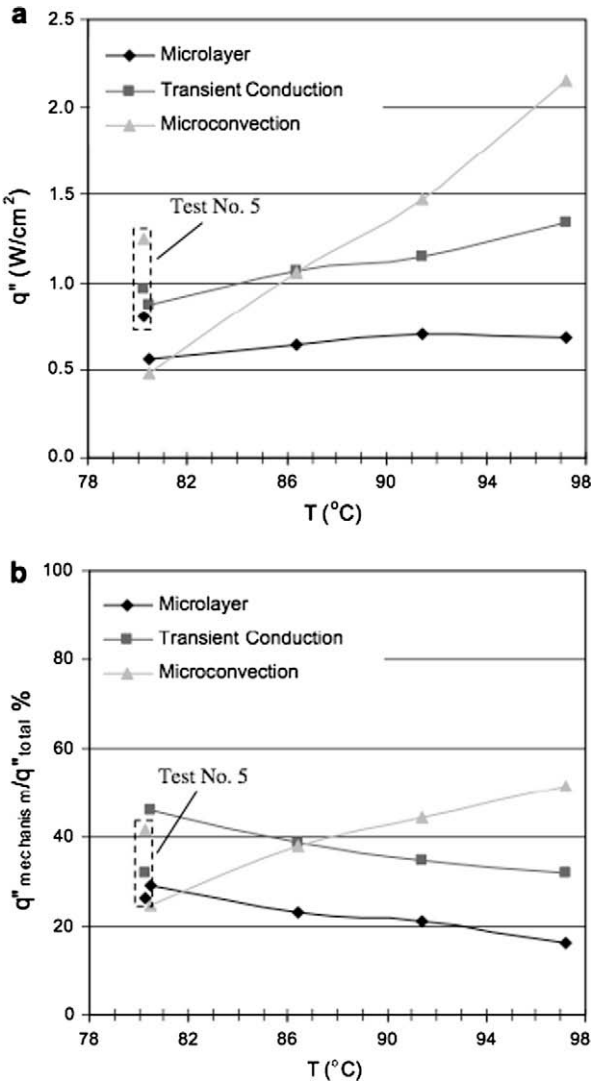

Fig. 8. Surface heat transfer contribution of various mechanisms: (a) heat transfer magnitude and (b) relative contribution. From Moghaddam and Kiger (2008).

heat must diffuse through the plate, complicating the interpretation of the temperature data. Due to the limitations and difficulties associated with liquid crystal use, researchers have generally moved to using infrared cameras.

3.4. Infrared camera data

Wagner and Stephan (2009) used an infrared camera to measure the temperature distribution on the backside of a 20 μm thick stainless steel heating foil during boiling of FC-84 (T_{sat} = 80 °C, 1 atm) and FC-3284 (T_{sat} = 50 °C, 1 atm) at 500 mbar and 950 mbar while imaging the bubble shape from the side. The local heat flux was obtained by performing an energy balance for each pixel taking into account the sensible heating, heat generation within the foil, heat conduction laterally within the foil, and heat lost to the fluid. Examples of heat transfer distributions are shown on Fig. 9. The total latent heat transferred into the bubble (Q_bub) was computed from changes in the bubble volume between time steps. The heat transferred through the microregion (Q_mic) was the wall heat transfer shown in Fig. 9, and could include microlayer evaporation, contact line heat transfer, transient conduction, and microconvection. Both Q_bub and Q_mic during are shown in Fig. 10. The heat transfer through the wall under the bubble for both cases between nucleation through bubble departure is about 22% of the total bubble latent heat, indicating most of the energy for bubble growth came from the only other source, the superheated liquid layer.

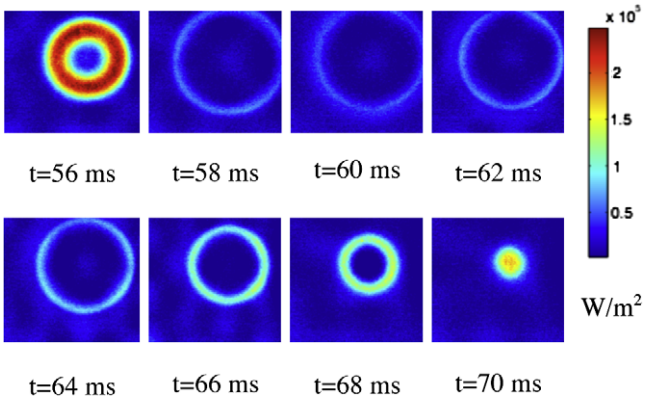

Fig. 9. Heat flux distribution during boiling of FC-3284 at 500 mbar, q = 1.29 W/cm^2. From Wagner and Stephan (2009).

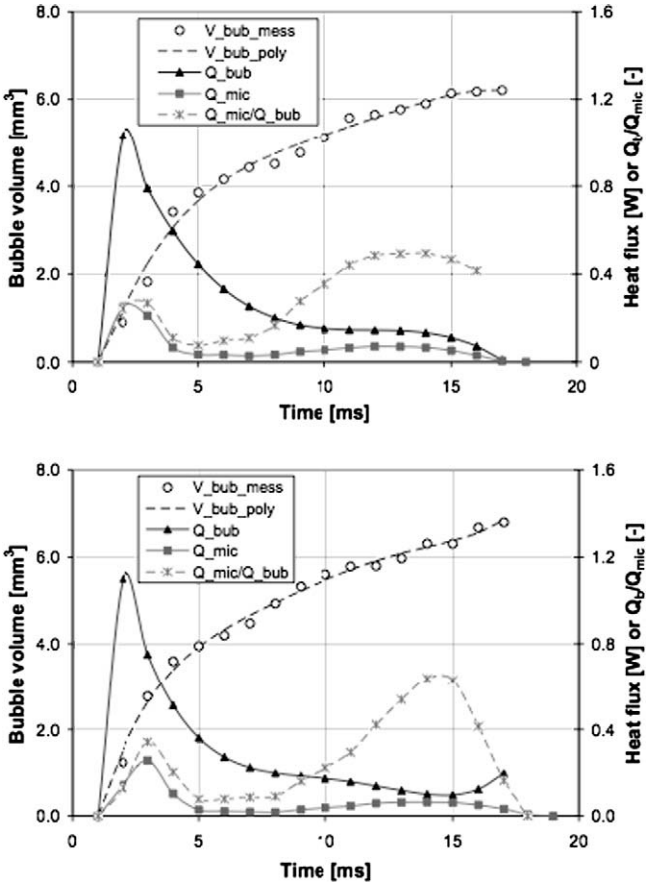

Fig. 10. Bubble volume and heat transfer vs. time, FC-84 at q = 12,000 W/m^2 (top) and FC-33284 at q = 12,900 W/m^2 (bottom). From Wagner and Stephan (2009).

3.5. Comparison with microlayer evaporation data

The recent experimental data discussed above indicates that microlayer evaporation does not play a dominant role in bubble heat transfer. This finding reinforces previous work in which

microlayer parameters were directly measured. Judd and Hwang (1976) used interferometric techniques to obtain time-resolved profiles of the microlayer during boiling of methylene chloride on an oxide coated glass surface. They found that the microlayer only contributed a small fraction of the wall heat transfer, especially at low heat fluxes. For example, for a bubble departure radius of 2.3 mm, the equivalent volume of fluid due to microlayer evaporation would have only produced a bubble of radius 0.26 mm at a heat flux of about 2.7 W/cm^2. When the heat flux was increased to 6 W/cm^2, the bubble departure radius decreased to 1.24 mm while the equivalent microlayer evaporation was only 0.18 mm. Later work by Fath and Judd (1978) found that decreasing the system pressure could increase the contribution of microlayer evaporation, but the contribution was still quite small (bubble departure radius of 1.4 mm vs. equivalent microlayer evaporation radius of 0.19 mm) at the lowest pressure and highest heat flux.

Koffman and Plesset (1983) obtained microlayer profiles during boiling of water and ethanol at a frame rate of 15,000 fps using a Fastax camera. The bubbles grew and lifted off the surface within a few milliseconds. The initial microlayer profile for ethanol (26.5 W/cm^2, 5.7 °C subcooling) had a thickness of 3 μm at a radius of 0.25 mm, and decreased by 2.2 μm/ms initially and at 1.25 μm/ms after about 1.4 ms. The heat removal rates were 138.5 W/cm^2 and 78.7 W/cm^2, respectively, but only occurred for a short time and over a small area. Similar data for water (20.4 W/cm^2, 21.7 °C subcooling) indicated evaporation rates of 1.04 μm/ms decreasing to 0.35 μm/ms after about 2 ms. The corresponding heat transfer was 226 W/cm^2 and 75.7 W/cm^2, respectively. They concluded that microlayer evaporation could not account for more than 50% of the bubble heat transfer, and that "microconvection must play at least an equal role".

4. Analysis

Liao et al. (2004) constructed a numerical model of bubble growth to predict the bubble growth rate in saturated pool boiling on a heater kept at constant tempeature. Both heat transfer through the microlayer and heat through the bubble dome were considered. The microlayer was assumed to have a linear profile whose slope was given by

$$\phi = \frac{C_2\sqrt{v_l t}}{R_b(t)} \tag{4}$$

as suggested by Cooper and Lloyd (1969). Their model was applied to simulate the bubble growth experimentally obtained by Yaddanapuddi and Kim (2001). In the early stage of bubble growth, heat transfer was primarily by microlayer evaporation, which enabled them to determine the value of C_2 in Eq. (4) to be 3.0. The heat transfer through the bubble cap depended on the thickness of the superheated liquid layer (d) surrounding the bubble. The value of d was found to be 30 mm through comparison with the heat transfer data. The model indicated that 70% of the heat gained by the bubble was through the bubble cap, which was consistent with the experimentally obtained results of Yaddanapuddi and Kim (2001).

5. Numerical simulations

Although many numerical simulations of bubble growth have been performed, the models were often built on an assumed heat transfer mechanism. For example, Lee and Nydahl (1989) performed a numerical simulation of bubble growth and departure, assuming that the bubble had the shape of a truncated sphere and a microlayer exists throughout the bubble growth period. Not surprisingly, they concluded that microlayer evaporation accounted for up to 87% of the heat transfer enhancement in nucleate boiling. Other numerical simulations made considerable simplifying assumptions (e.g., 2-D cylindrical bubbles in Son 2001 and Bai and Fujita 1999), and are therefore not considered in this review. Still other papers simulate the bubble growth and departure process and compare with experimental results, but do not discuss the relative contributions of the heat transfer mechanisms (e.g., Bai and Fujita 2000; Mukherjee and Kandlikar 2007). The papers reviewed below simulated bubble growth with a minimum of simplifying assumptions for realistic bubble geometries with a focus on identifying the relevant heat transfer mechanisms.

Son et al. (1999) performed a numerical simulation of the growth and departure of bubbles during boiling of water using a level-set method. The computational domain was divided into macro (bubble and liquid surrounding the bubble) and micro (thin liquid film between bubble and wall) regions. The thickness of the adsorbed liquid layer was assumed to be 6×10^{-10} m, the contact angle was fixed at 38°, and the initial size of the bubble was assumed to be four times the mesh size. The waiting time was obtained from experiment. The heat transfer contribution from the microregion was found to be about 20%. Similar results for vertical merger of two and three bubbles were obtained by Son et al. (2002), and are shown in Fig. 11. The heat transfer contribution from the microregion was found to be about 15–20% of the total heat transfer for the three bubble growth and merger patterns. The variation in Nu vs. time is quite different from what has been obtained experimentally, however, and may indicate that some of the heat transfer mechanisms were not modeled properly.

Fuchs et al. (2006) also performed numerical simulations of bubble growth and departure including wall conduction effects with special emphasis on the evaporating meniscus. The waiting time between successive bubbles was specified as an input parameter. A spherical bubble shape was assumed for the bubble cap during the bubble growth process from an initial bubble of diameter of 3 μm, while a free deformable surface was assumed once the bubble departed. The apparent contact angle during bubble growth was obtained from a model of the microregion (Kern and Stephan 2003) and the accommodation coefficient was assumed to be the maximum value of unity. Time dependent heat transfer profiles through various interfaces (Fig. 12) indicate that the heat transfer through the bubble cap (interface 5 or 6) and between the wall and the bulk liquid in the macro-region (interface 2) each account for about 44% of the total bubble heat transfer. Only 12% of the total heat transfer occurs through the thin-film microregion at the three-phase contact line (interface 3)[1]. The heat transfer through interface 3 is likely to be much smaller in real systems since the accommodation coefficient is generally significantly smaller than unity.

Mukherjee and Kandlikar (2006) numerically computed the heat transfer associated with the advancing and receding contact angle in an evaporating meniscus on a heated copper surface. Good agreement with experiments (Kandlikar et al., 2005) were obtained. They observed that the heat transfer coefficient at the advancing meniscus was considerably higher than at the receding meniscus even though the contact angle for the receding meniscus was much smaller.

6. Effect of fluid properties

The experimental results described above may only be applicable to the narrow range of fluids tested (FC-72, FC-84, and FC-33284). The heat of vaporization for these fluids can be quite low compared with the specific heat, so the impact of microlayer

[1] Interface 3 in Fuchs et al. (2006) corresponds to q_{cl} in this paper.

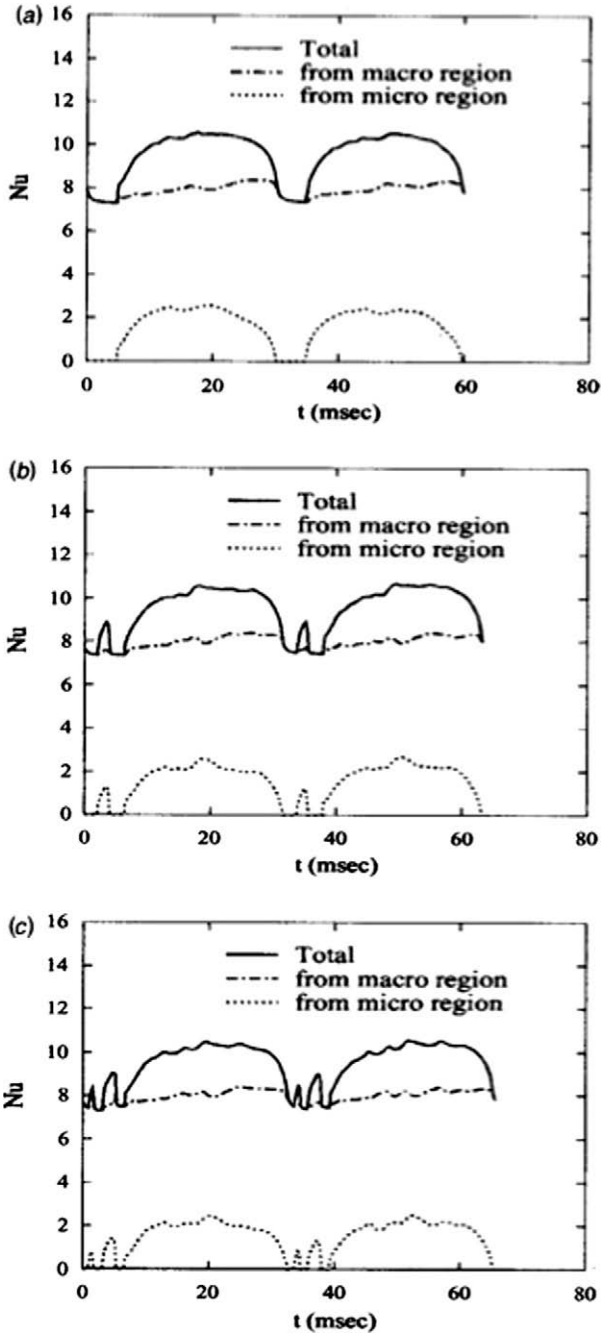

Fig. 11. Variation in Nusselt number for $\Delta T = 10$ K and three waiting periods: (a) 4.8 ms, single bubble (b) 2.4 ms, vertical merger of two bubbles, and (c) 1.28 ms, vertical merger of three bubbles. From Son et al. (2002).

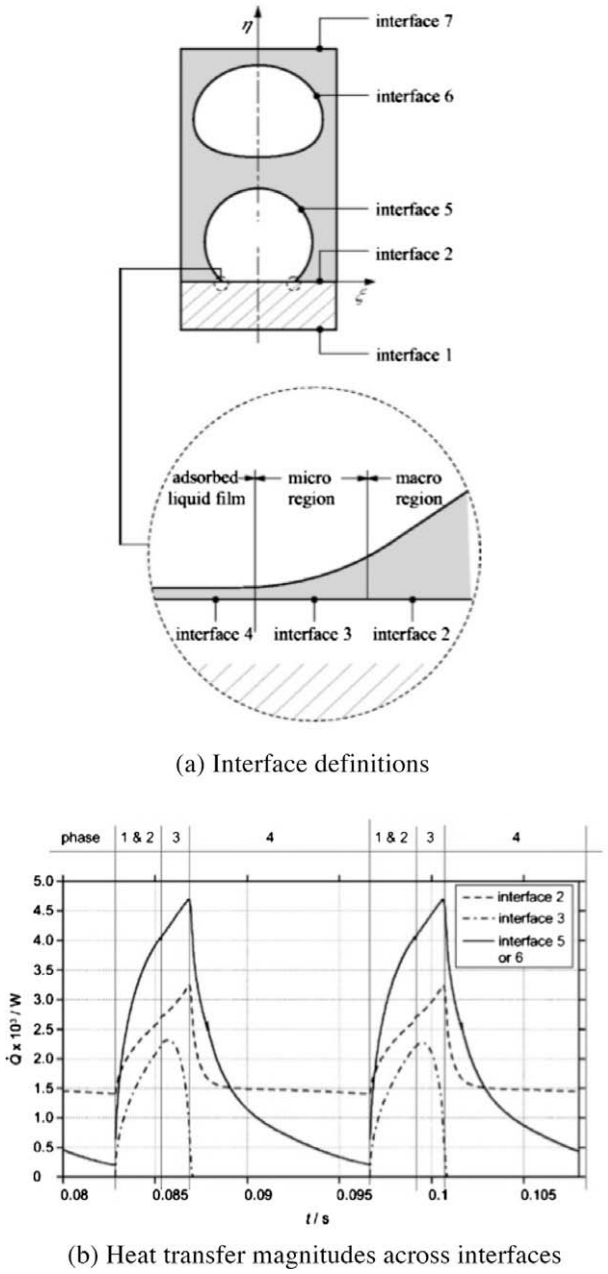

Fig. 12. Definition of interfaces and the heat transfer across them (propane/*n*-butane, $p_r = 0.2$, $T_w - T_{sat} = 8.7$ K, $x_{L,1} = 0.245$). Phases 1 and 2 correspond to the bubble growth process, phase 3 corresponds to the bubble detachment period when liquid rewets the wall, and phase 4 is the waiting time after bubble departure. From Fuchs et al. (2006).

evaporation may be lower than for other fluids. The Jakob number, defined as

$$Ja = c_p(T_w - T_{sat})/h_{fg} \tag{5}$$

is a measure of the sensible heat to the heat of vaporization. A summary of the *Ja* values for the experimental work discussed above shown in Table 1 indicates that the sensible heating is quite large compared to the heat of vaporization. The fluids used by Cooper and Lloyd (1969) have significantly lower *Ja* than the FC fluids, and may be a reason they observed a large microlayer heat transfer. Results using other fluids with much larger heats of vaporization have recently become available to test this hypothesis.

Delgoshaei and Kim (2009) obtained measurements of bubble growing on a microheater array using pentane under near saturated conditions ($T_{bulk} = 31.6$ °C, $T_{sat} = 35.8$ °C, Pressure = 101 kPa). Pentane has a Jakob number similar to the toluene and isopropyl alcohol used by Cooper and Lloyd (1969). Their observations indicate that the physical size of the bubble was significantly larger than what could be accounted for by the wall heat transfer, consistent with the results with the FC fluids (Fig. 13).

Gerardi et al. (2009) obtained boiling measurements with water on a sapphire wafer coated with an indium tin oxide (ITO) heater. A high-speed infrared camera was used to measure the temperature distribution at the solid–liquid interface while a visible light camera was used to image the bubble growth and departure. The Jakob

Table 1
Summary of Jakob number calculation for experimental data.

Study	Fluid	C_p (kJ/kg K)	H_{fg} (kJ/kg)	$T_{wall}-T_{sat}$ (°C)	Ja
Demiray and Kim (2004)	FC-72	1.10	88.0	19	0.24
Myers et al. (2005)	FC-72	1.10	88.0	38–50	0.48–0.62
Wagner and Stephan (2009)	FC-84	1.10	90.0	21.1	0.26
Wagner and Stephan (2009)	FC-3284	1.10	105.0	19.8	0.21
Cooper and Lloyd (1969)	Toluene	1.69	350.0	17–33	0.08–0.16
Cooper and Lloyd (1969)	Isopropyl Alcohol	2.57	667.0	42	0.16
Delgoshaei and Kim (2009)	Pentane	2.37	357.8	16.2–20.2	0.11–0.13
Gerardi et al. (2009)	Water	4.18	2257	9	0.017

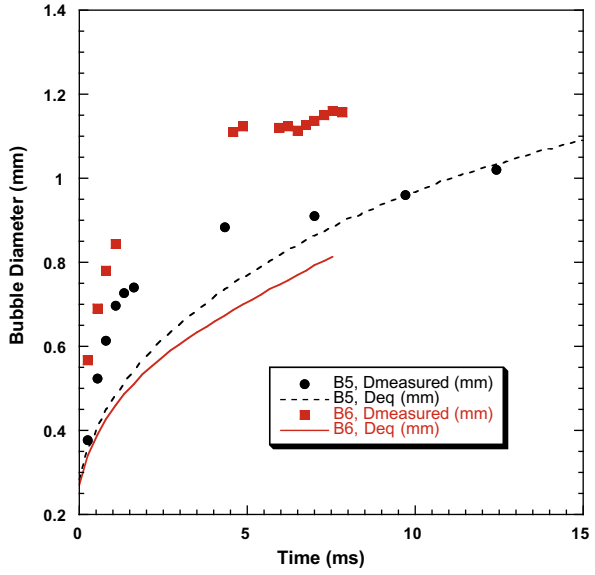

Fig. 13. Measured and equivalent bubble diameters for boiling of pentane. From Delgoshaei and Kim (2009).

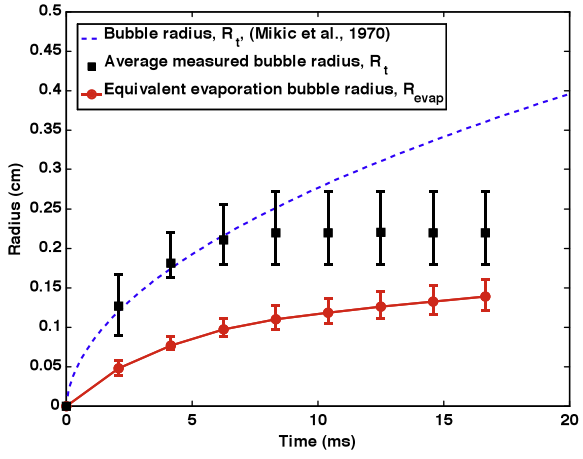

Fig. 14. Measured and equivalent bubble radii for boiling of water. From Gerardi et al. (2009).

number for water is an order of magnitude smaller than any of the fluids discussed above, yet they also observed a physical bubble radius that was much larger than the equivalent bubble radius obtained from wall heat transfer measurements (Fig. 14).

The data for fluorinerts, pentane, and water all indicate that heat is gained by the bubble mainly through the bubble cap. The dominant bubble heat transfer mechanism does not appear to be dependent on the fluid properties.

7. Summary and conclusions

The recent experimental work performed using a wide array of techniques by independent researchers along with recent numerical and analytical work clearly indicates that the dominant mechanism by which heat is transferred by isolated bubbles during boiling is through transient conduction and/or microconvection. Heat transfer through microlayer evaporation and contact line heat transfer do not account for more than approximately 25% of the overall heat transfer and often substantially less.

It is also clear that none of the proposed bubble heat transfer models described in the Introduction are consistent with the experimentally observed heat transfer signatures. Contrary to what would be expected from the transient conduction model of Mikic and Rohsenhow (1969), a large heat transfer by transient conduction is observed *during* the wall rewetting process *before* the bubble actually departs, not only during regrowth of the superheated liquid layer after bubble departure. The heat transfer is also not spatially uniform as their model suggests, and the area of influence of the departing bubble is much smaller than twice the departure diameter assumed in the model.

Although the formation of a microlayer between the bubble and the heated wall was observed in many cases and was accompanied by large heat transfer rates, the duration was not nearly long enough or large enough to account for the physical size of the bubble, indicating that the bubble gained the great majority of its energy for growth through the bubble cap and not from processes at the wall. The heat transfer during the liquid rewetting process during bubble departure was also observed to be significantly larger in many cases than during microlayer evaporation.

The contact line heat transfer model is lacking for similar reasons. Extremely high heat transfer rates at the three-phase contact line would have been expected as the microlayer dried out, but higher local heat transfer was often observed during rewetting of the dry area during bubble departure.

All of the above mechanisms contribute to the overall bubble heat transfer to varying degrees. At present, a single model incorporating these submodels is currently not available. Future models of boiling should be constructed based on the proper physics clarified by the recent experimental data.

Acknowledgement

This work was supported by NASA Grant No. NNX08AI60A. The grant monitor was Mr. John McQuillen.

References

Bai, Q., Fujita, Y., 1999. Numerical simulation of the growth for a single bubble in nucleate boiling. Therm. Sci. Eng. 7 (4), 45–53.
Bai, Q., Fujita, Y., 2000. Numerical simulation of bubble growth in nucleate boiling – effects of system parameters. Multiphase Sci. Technol. 12 (3&4).

Bayazit, B.B., Hollingsworth, D.K., Witte, L.C., 2003. Heat transfer enhancement caused by sliding bubbles. J. Heat Transfer 125 (3), 503–509.
Cooper, M.G., Lloyd, A.J.P., 1969. The microlayer in nucleate boiling. Int. J. Heat Mass Transfer 12, 895–913.
Delgoshaei, P., Kim, J., 2009. Microscale heat transfer measurements during subcooled pool boiling of pentane. In: Proceedings of the 2009 Summer Heat Transfer Conference, San Francisco, July 19–23.
Demiray, F., Kim, J., 2004. Microscale heat transfer measurements during pool boiling of FC-72: effect of subcooling. Int. J. Heat Mass Transfer 47, 3257–3268.
Fath, H.S., Judd, R.L., 1978. Influence of system pressure on microlayer evaporation heat transfer. J. Heat Transfer 100, 49–55.
Forster, H.K., Greif, R., 1959. Heat transfer to a boiling liquid – mechanisms and correlations. J. Heat Transfer 81, 45.
Forster, H.K., Zuber, N., 1955. Dynamics of vapor bubbles and boiling heat transfer. AICHE J. 1, 531.
Fuchs, T., Kern, J., Stephan, P., 2006. A transient nucleate boiling model including microscale effects and wall heat transfer. J. Heat Transfer 128, 1257–1265.
Gerardi, C., Buongiorno, J., Hu, L. W., McKrell, T., 2009. Measurement of nucleation site density, bubble departure diameter and frequency in pool boiling of water using high-speed infrared and optical cameras. In: Proceedings of 7th ECI International Conference on Boiling Heat Transfer, Florianópolis, Brazil, May 3–7.
Han, C.Y., Griffith, P., 1965. The mechanism of heat transfer in nucleate pool boiling. Int. J. Heat Mass Transfer 8, 887–914.
Hendricks, R.C., Sharp, R.R., 1964. Initiation of cooling due to bubble growth on a heating surface. NASA TN D2290.
Hsu, Y.Y., 1962. On the size range of active nucleation cavities on a heating surface. J. Heat Transfer 84, 207–213.
Judd, R.L., Hwang, K.S., 1976. A comprehensive model for nucleate pool boiling heat transfer including microlayer evaporation. J. Heat Transfer, 623–629.
Kandlikar, S.G., Kuan, W.K., Mukherjee, A., 2005. Experimental study of heat transfer in an evaporating meniscus on a moving heated surface. J. Heat Transfer 127, 244–252.
Kenning, D.B.R., Kono, T., Wienecke, M., 2001. Investigation of boiling heat transfer by liquid crystal thermography. Exp. Therm. Fluid Sci. 25, 219–229.
Kern, J., Stephan, P., 2003. Theoretical model for nucleate boiling heat and mass transfer of binary mixtures. J. Heat Transfer 125, 1106–1115.
Kim, J., Oh, B.D., Kim, M.H., 2006. Experimental study of pool temperature effects on nucleate pool boiling. Int. J. Multiphase Flow 32, 208–231.
Koffman, L.D., Plesset, M.S., 1983. Experimental observations of the microlayer in vapor bubble growth on a heated solid. J. Heat Transfer 105, 625–632.
Lee, H.C., Oh, B.D., Bae, S.W., Kim, M.H., Lee, J.Y., Song, I.S., 2003a. Partial nucleate boiling on the microscale heater maintaining constant wall temperature. J. Nucl. Sci. Technol. 40 (10), 768–774.
Lee, H.C., Oh, B.D., Bae, S.W., Kim, M.H., 2003b. Single bubble growth in saturated pool boiling on a constant wall temperature surface. Int. J. Multiphase Flow 29, 1857–1874.
Lee, R.C., Nydahl, J.E., 1989. Numerical calculations of bubble growth in nucleate boiling from inception through departure. J. Heat Transfer 111, 474–479.
Liao, J., Mei, R., Klausner, J.F., 2004. The influence of the bulk liquid thermal boundary layer on saturated nucleate boiling. Int. J. Heat Mass Transfer 25, 196–208.
Mikic, B.B., Rohsenhow, W.M., 1969. A new correlation of pool boiling data including the effect of heating surface characteristics. J. Heat Transfer 9, 245–250.
Moghaddam, S., Kiger, K., 2008. Physical mechanisms of heat transfer during single bubble nucleate boiling of FC-72 under saturated conditions – I. Experimental investigation. Int. J. Heat Mass Transfer.
Moore, F.D., Mesler, R.B., 1961. The measurement of rapid surface temperature fluctuations during nucleate boiling of water. AICHE J. 7, 620–624.
Mukherjee, A., Kandlikar, S.G., 2006. Numerical study of an evaporating meniscus on a moving heated surface. J. Heat Transfer 128, 1285–1292.
Mukherjee, A., Kandlikar, S.G., 2007. Numerical study of single bubbles with dynamic contact angle during nucleate pool boiling. Int. J. Heat Mass Transfer 50, 127–138.
Myers, J.G., Yerramilli, V.K., Hussey, S.W., Yee, G.F., Kim, J., 2005. Time and space resolved wall temperature and heat flux measurements during nucleate boiling with constant heat flux boundary conditions. Int. J. Heat Mass Transfer 48 (12), 2429–2442.
Rosenhow, W.M., 1952. A method of correlating heat transfer data for surface boiling of liquids. Trans. ASME 4, 969–975.
Snyder, N.R., Edwards, D.K., 1956. Summary of confrence on bubble dynamics and boiling heat transfer. Memo 20-137, Jet Propulsion Laboratory, June 14–15.
Sodtke, C., Kern, J., Stephan, P., 2006. High resolution measurements of wall temperature distribution underneath a single vapor bubble under microgravity conditions. Int. J. Heat Mass Transfer 49, 1100–1106.
Son, G., 2001. Numerical study on a sliding bubble during nucleate boiling. KSME J. 15 (7), 931–940.
Son, G., Dhir, V.K., Ramanujapu, N., 1999. Dynamics and heat transfer associated with a single bubble during nucleate boiling on a horizontal surface. J. Heat Transfer 121, 623–631.
Son, G., Ramanujapu, N., Dhir, V.K., 2002. Numerical simulation of bubble merger process on a single nucleation site during pool nucleate boiling. J. Heat Transfer 124, 51–62.
Stephan, P., Hammer, J., 1994. A new model for nucleate boiling heat transfer. Warme und Stoffubertragung 30, 119–125.
Tien, C.L., 1962. A hydrodynamic model for nucleate pool boiling. Int. J. Heat Mass Transfer 5, 540–553.
Van Stralen, S.J.D., 1966a. The mechanisms of nucleate boiling in pure liquids and in binary mixtures – Part I. Int. J. Heat Mass Transfer 9, 995–1020.
Van Stralen, S.J.D., 1966b. The mechanisms of nucleate boiling in pure liquids and in binary mixtures – Part II. Int. J. Heat Mass Transfer 9, 1021–1046.
Van Stralen, S.J.D., 1967. The mechanisms of nucleate boiling in pure liquids and in binary mixtures – Part III. Int. J. Heat Mass Transfer 10, 1469–1498.
Wagner, E., Stephan, P., in press. High resolution measurements at nucleate boiling of pure FC-84 and FC-32384 and its binary mixtures. J. Heat Transfer.
Watwe, A.A., Hollingsworth, D.K., 1994. Liquid crystal thermal images of surface temperature during incipient pool boiling. J. Exp. Therm. Fluid Sci. 9, 22–33.
Wayner, P.C., Kao, Y.K., LaCroix, L.V., 1976. The interline heat transfer coefficient on an evaporating wetting film. Int. J. Heat Mass Transfer 19, 487–492.
Yaddanapuddi, N., Kim, J., 2001. Single bubble heat transfer in saturated pool boiling of FC-72. Multiphase Sci. Technol. 12 (3–4), 47–63.
Zuber, N., 1963. Nucleate boiling the region of isolated bubbles and the similarity with natural convection. Int. J. Heat Mass Transfer 6, 53–78.